Recurrent network activity drives striatal synaptogenesis

Published in final edited form as:
Nature. ; 485(7400): 646–650. doi:10.1038/nature11052.

Recurrent network activity drives striatal synaptogenesis

Yevgenia Kozorovitskiy[1,3], **Arpiar Saunders**[1,3], **Caroline A. Johnson**[1], **Bradford B. Lowell**[2], and **Bernardo L. Sabatini**[1]

[1]Howard Hughes Medical Institute, Department of Neurobiology, Harvard Medical School

[2]Endocrinology Division, Beth Israel Deaconess Medical Center

Abstract

Neural activity during development critically shapes postnatal wiring of the mammalian brain. This is best illustrated by the sensory systems, in which the patterned feed-forward excitation provided by sensory organs and experience drives the formation of mature topographic circuits capable of extracting specific features of sensory stimuli[1,2]. In contrast, little is known about the role of early activity in the development of the basal ganglia, a phylogenetically ancient group of nuclei fundamentally important for complex motor action and reward-based learning[3,4]. These nuclei lack direct sensory input and are only loosely topographically organized[5,6], forming interlocking feed-forward and feed-back inhibitory circuits without laminar structure. Here we use transgenic mice and viral gene transfer methods to modulate neurotransmitter release and neuronal activity *in vivo* in the developing striatum. We find that the balance of activity among the two inhibitory and antagonist pathways in the striatum regulates excitatory innervation of the basal ganglia during development. These effects indicate that the propagation of activity through a multi-stage network regulates the wiring of the basal ganglia, revealing an important role of positive feedback in driving network maturation.

Excitatory input from the cortex and thalamus enters the basal ganglia (BG) through the striatum, where it is locally processed and transformed into two inhibitory, GABAergic outputs called the direct and indirect pathways[7]. Each pathway arises from a distinct class of spatially intermixed medium spiny neurons (MSNs) with differing projections and molecular characteristics[8]. These projection patterns suggest opponent effects on BG output: direct pathway MSNs synapse in Substantia Nigra reticulata (SNr), the BG output nucleus, whereas indirect pathway MSNs synapse in Globus Pallidus (GP), which in turn inhibits the SNr[9]. Since the SNr provides GABAergic inhibition to the thalamus, which subsequently activates cortex through glutamatergic synapses, the interactions of BG, thalamus and cortex can be simplified as a closed loop, differentially controlled by the direct and indirect pathways (Supplementary Figure 1). Anatomical evidence supports this model[10,11] and the opponent roles of the two pathways on motor behavior have been recently demonstrated in adult rodents[12,13]. In addition, *in vivo* recordings and circuit tracing indicate that different corticostriatal inputs are processed through segregated, parallel networks[6,10,11,14]. Given this organization, establishing correct wiring of the cortex-BG-thalamus circuitry poses a significant developmental challenge, requiring that functional interactions be maintained over polysynaptic networks comprised of mixed inhibitory and excitatory projections.

Correspondence: bsabatini@hms.harvard.edu.
[3]equal contribution.

Author Contribution

Y.K., A.S. and B.L.S designed the experiments. Y.K. and A.S. performed experiments and analyzed data. C.A.J assisted in experiments and genotyping. B.B.L. generated the conditional *Slc32a1* mouse. Y.K., A.S. and B.L.S wrote the paper with contributions from C.A.J. and B.B.L.

To investigate how striatal activity contributes to circuit development, we generated mice incapable of releasing GABA from direct or indirect pathway MSNs through conditional knockout of *Slc32a1*, which encodes the vesicular GABA transporter (vgat) (Figure 2)[15]. GABAergic neurons lacking vgat are unable to package GABA into synaptic vesicles for release[16, 17]. Pathway specificity was conferred by BAC transgenic mice that express Cre recombinase under the control of the type 1a or type 2 dopamine receptors[18]. In *Drd1a* Cre (D1-Cre) mice, Cre expression in GABAergic neurons is largely limited to direct pathway MSNs, although Cre is also found in non-GABAergic cortical neurons (Figure 1a, Supplementary Figures 2–3). In *Drd2* Cre (D2-Cre) mice, Cre expression is largely limited to indirect pathway MSNs (Figure 1a, Supplementary Figure 2). Mice with *Slc32a1* deletion in direct or indirect pathway MSNs showed opposing locomotor phenotypes and survived until weaning (Supplementary Figure 4), a time of increasing reliance on reward-based complex motor actions.

To test the efficacy of silencing of GABA release we relied on optogenetic analysis of MSN-to-MSN collateral synapses[19]. Channelrhodopsin2-mCherry fusion protein (ChR2-mCherry) was expressed in Cre-positive MSNs by injecting an adeno-associated virus (AAV) containing a double floxed inverted ChR2-mCherry transgene into the striatum at P3-5 (Figure 1b)[20]. Whole-cell voltage-clamp recordings of ChR2-negative MSNs demonstrated light-evoked GABAergic currents in acute brain slices from P13-18 *D1-Cre; Slc32a1*$^{f/+}$ mice (−1477 ± 352 pA, n=20) and *D2-Cre; Slc32a1*$^{f/+}$ (−1319 ± 221 pA, n=12), which were absent in littermate *Slc32a1*$^{f/f}$ animals (*D1-Cre; Slc32a1*$^{f/f}$: −2.19 ± 1.6 pA, n=7; *D2-Cre; Slc32a1*$^{f/f}$: −9.91 ± 2.4 pA, n=7) (Figure 1c, Supplementary Figure 5).

We examined whether GABA release from MSNs is required for cell survival and long-range axonal projections. The proportion of Cre^{+} cell nuclei was 45–48% in D1-Cre and D2-Cre animals and independent of the number of conditional *Slc32a1* alleles (Supplementary Figure 6). MSNs lacking GABA release form qualitatively normal long-range axonal projections, based on examination of ChR2-mCherry fluorescence in the SNr and GP (SNr, 18–19% and GP, 15–16% fractional area coverage) (Supplementary Figure 7). These observations confirm that MSNs lacking GABA release are maintained in normal numbers and extend grossly normal axons.

In contrast, silencing GABA release had profound consequences for the number of excitatory synapses received, which are typically associated with dendritic spines[21,22]. In the rodent striatum, inhibitory synapse density is relatively constant throughout postnatal development, while excitatory synapse density rises dramatically between P10 and P21[23]. Therefore, we restricted analyses to pairs of littermate control and *Slc32a1* null mice at P14-15. We identified MSNs of each pathway using ChR2-mCherry expression delivered by either Cre-On or Cre-Off AAVs (Supplementary Figure 8a)[24]. Even within this narrow developmental window, we detected an increase in miniature excitatory postsynaptic current (mEPSC) frequencies, but not amplitudes, among same genotype littermates (frequency, P14: 0.14 ± 0.06 Hz, P15: 0.34 ± 0.1 Hz; amplitude, P14: 14.4 ± 1.0 pA, P15: 13.9 ± 0.4 pA) (Supplementary Figure 8b). In mice lacking GABA release in direct pathway MSNs, mEPSC frequency was reduced in both direct and indirect pathway MSNs compared to heterozygous sibling controls (direct pathway MSNs, *D1-Cre;Slc32a1*$^{f/+}$: 0.22 ± 0.04 Hz, n=18, *D1-Cre Slc32a1*$^{f/f}$: 0.08 ± 0.02 Hz, n=16; indirect pathway MSNs, *D1-Cre Slc32a1*$^{f/+}$: 0.32 ± 0.07 Hz, n=14, *D1-Cre;Slc32a1*$^{f/f}$: 0.1 ± 0.03 Hz, n=15) (Figure 2a, c). Conversely, mEPSC frequency was increased in MSNs of mice with output-silenced indirect pathway (direct pathway MSNs, *D2-Cre;Slc32a1*$^{f/+}$: 0.11 ± 0.04 Hz, n=9, *D2-Cre;Slc32a1*$^{f/f}$: 0.28 ± 0.07 Hz, n=6; indirect pathway MSNs, *D2-Cre;Slc32a1*$^{f/+}$: 0.15 Hz ± 0.06, n=5, *D2-Cre;Slc32a1*$^{f/f}$: 0.37 Hz ± 0.04, n=14) (Figure 2b, d). mEPSC amplitudes were largely unaffected by either manipulation (Supplementary Figure 8c-d).

Changes in mEPSC rates were paralleled by alterations in dendritic spine density, indicating concurrent changes in structural and functional correlates of excitatory synapse number. Dendritic spine density of all MSNs was decreased by silencing the direct pathway and increased by silencing the indirect pathway (D1-Cre, direct pathway, 0.84 ± 0.03 spines/μm vs. 0.45 ± 0.05, n=6 and 7; D1-Cre, indirect pathway, 0.68 ± 0.05 spines/μm vs. 0.41 ± 0.02, n=5/group; D2-Cre, indirect pathway, 0.56 ± 0.03 spines/μm vs. 1.02 ± 0.05, n=5 and 6; D2-Cre, direct pathway, 0.41 ± 0.02 spines/μm vs. 0.63 ± 0.08 n=6/group) (Figure 2). Together these data show that the degree of excitatory innervation of MSNs is determined by striatal output, such that excitatory hypo- or hyper-innervation is triggered by silencing direct or indirect pathway, respectively.

Complementary, pathway-dependent effects on excitatory input could be due to cell-intrinsic differences in direct and indirect pathway MSNs. Alternatively, common activity-dependent wiring rules could be differentially activated by each perturbation of BG output. For example, a net increase in SNr inhibitory output, caused by silencing direct pathway MSNs, could diminish thalamic and cortical activity, decreasing glutamate release and glutamatergic synapse formation in the striatum. In contrast, silencing the indirect pathway could have the converse set of effects (Supplementary Figure 1b-d). The observation that direct or indirect pathway MSNs show similar perturbations despite selective deletion of *Slc32a1* only in MSNs of the Cre-expressing pathway (Figure 2) provides support for the circuit-level model.

To test for cell-autonomous, *Slc32a1*-dependent regulation of glutamatergic innervation, we deleted *Slc32a1* in a small and sparse subpopulation of striatal neurons by injecting small quantities of AAV encoding Cre-mCherry into *D2-GFP;Slc32a1*$^{f/f}$ mice at P0-1 (Supplementary Figure 9a-b). Analysis of mEPSCs and dendritic spines in neighboring Cre^{+} and Cre^{-} MSNs (identified by nuclear mCherry fluorescence) belonging to the direct and indirect pathway (identified by GFP expression) revealed no changes in mEPSC frequency or dendritic spine density (Supplementary Figure 9c-e). Thus, *Slc32a1*-dependent, cell-intrinsic mechanisms are unlikely to contribute to differential effects on glutamatergic innervation seen with silenced direct or indirect pathways.

We examined the consequences of manipulating striatal activity specifically during the period of striatal excitatory synaptogenesis[23] using the RASSL (G-protein-coupled receptor activated solely by a synthetic ligand) hM4D[25,26] in direct or indirect pathway MSNs (Figure 3). hM4D is activated by a blood-brain-barrier permeable molecule clozapine-n-oxide (cno), allowing non-invasive *in vivo* manipulation of neural activity. hM4D couples to the $G\alpha_{i/o}$ pathway, which reduces action potential firing in many cell types (Supplementary Figure 10) by activating K^{+} channels[13]. AAV carrying the double floxed inverted hM4D-mCherry transgene[26] was injected in D1- or D2-Cre mice at P0-1 and, starting at P8, cno (1 mg/kg) or saline were administered subcutaneously 2×/day to littermate pups. Consistent with our hypothesis, animals with large bilateral injections of AAV to dampen activity of many direct or indirect pathway MSNs, respectively, down- or up-regulated mEPSC frequency and dendritic spine density, relative to saline-injected littermates (direct pathway MSNs: frequency, 0.8 ± 0.1 Hz vs. 0.36± 0.07 Hz, n=18 and 25; spine density 0.96 ± 0.04 spines/μm vs. 0.49 ± 0.05 spines/μm, n=5/group; indirect pathway MSNs: frequency, 0.04 ± 0.01 Hz vs. 0.27 ± 0.09 Hz, n=7 and 8; spine density, 0.54 ± 0.05 spines/μm vs. 0.98 ± 0.06 spines/μm, n=5/group) (Figure 3a-c, Supplementary Figure 12a). Similar results were observed with the *Adora2a-Cre* mouse, based on the adenosine 2A receptor promoter, another Cre driver line for indirect pathway MSNs (Supplementary Figure 11).

In contrast, sparse, unilateral hM4D delivery aimed to minimally impact circuit dynamics, did not alter mEPSC frequency and dendritic spine density in hM4D-expressing neurons

relative to uninfected neighboring MSNs of the same pathway (Figure 3d-f, Supplementary Figure 12b). These data also indicate that hM4D-mediated perturbation of G-protein-coupled intracellular signaling pathways is not responsible for the changes in excitatory synapses.

Three lines of evidence – analyses of non-manipulated MSNs in pathway specific conditional *Slc32a1* knockouts, of sparse *Slc32a1* null MSNs, and of the effects of widespread vs. sparse hM4d manipulation of neural activity – support the hypothesis that circuit-level patterns of activity, rather than cell-intrinsic mechanisms, determine the degree of glutamatergic innervation of striatal MSNs. Inherent to this proposed mechanism is the assumption that the BG output modulates corticostriatal or thalamostriatal glutamatergic activity, which, in turn, regulates excitatory synaptogenesis in the striatum. To probe this mechanism, we directly tested (1) the ability of glutamate exposure to drive spinogenesis in the striatum and (2) the effect of manipulating corticostriatal activity on striatal spinogenesis and synaptogenesis.

To test whether glutamate release in the striatum is sufficient to induce spinogenesis, we focally stimulated aspiny segments of P8-11 MSN dendrites with 2-photon laser uncaging of glutamate[27]. Sparse viral delivery of Cre was used to activate TdTomato reporter fluorescence in a small subset of MSNs in *D2-GFP;Ai14-lsl-TdTomato* mice. 2-photon laser-scanning microscopy was used to monitor dendritic structure during glutamate stimulation (Figure 4a-b). Stimulation power was calibrated to evoke moderate ~7 pA currents from existing spines (Supplementary Figure 13). Using protocols that robustly induce synaptogenesis in layer 2/3 pyramidal neurons of developing cortex[27], we observed growth of a new dendritic spine at the glutamate uncaging site in ~50% of trials. The probability of spine growth was similar in direct and indirect pathway MSNs (Figure 4c), was unaffected by blockade of $GABA_A$ receptors (52% and 50% success percentage for GFP+ and GFP− MSNs in control conditions, and 56% and 51%, respectively, in $GABA_A$ antagonist), and matched prior results in cortical pyramidal cells[27]. Thus, glutamatergic stimulation is sufficient to drive spinogenesis in the developing striatum.

To test whether the postnatal activity of corticostriatal projections drives synaptogenesis, we used the *Rbp4-Cre* mouse line to express hM4D in corticostriatal neurons emanating from deep cortical layers (Figure 4c, *left*). *Rbp4-Cre;D2-GFP* mice were injected with the double floxed inverted AAV carrying hM4D-mCherry at P0-1 and, starting at P8, cno (1 mg/kg) or saline were administered subcutaneously 2×/day to littermate pups. For MSNs of both pathways assayed at P14-15, mEPSC frequency and spine density were decreased after cno treatment, with no change in mEPSC amplitude (direct pathway MSNs: frequency, 0.66 ± 0.2 Hz vs. 0.25 ± 0.05 Hz, n=12 and 9; spine density 0.60 ± 0.05 spines/μm vs. 0.38 ± 0.03 spines/μm, n=7 and 6; indirect pathway MSNs: frequency, 0.65 ± 0.14 Hz vs. 0.25 ± 0.04 Hz, n=16 and 16; spine density, 0.58 ± 0.03 spines/μm vs. 0.31 ± 0.02 spines/μm, n=7 and 6) (Figure 4e). Since inhibition of Rbp4-Cre^+ corticostriatal projections caused no change in locomotion at P14-15 (Supplementary Figure 14), activity-dependent control of striatal synaptogenesis is not secondary to behavioral changes.

To determine whether activity-dependent changes in striatal synaptogenesis persist into early adulthood, we inhibited the activity of corticostriatally projecting Rbp4-Cre neurons during P8-P15 and examined excitatory innervation in indirect pathway MSNs at P25-28 (Figure 4f). Both mEPSC frequency and spine density were reduced in cno-treated mice, compared to saline injected controls (indirect pathway MSNs: frequency, 0.73 ± 0.12 Hz vs. 0.29 ± 0.07 Hz, n=28 and 26; spine density, 0.83 ± 0.02 spines/μm vs. 0.64 ± 0.02 spines/μm, n=10/group) (Figure 4g-h). Thus, perturbations of cortex-BG-thalamus circuit activity in early life can have lasting effects into adulthood.

Our data reveal that the balance of activity in direct/indirect pathways dictates postnatal excitatory innervation of the striatum. Since manipulating striatal output alters the structure of its input, activity must act recurrently, through a polysynaptic, multi-stage circuit. The simplest explanation for these findings is that glutamate release from cortical and thalamic axons in the striatum promotes the formation or stabilization of glutamatergic synapses onto MSNs. Perturbations that result in relative activation of the direct pathway compared to the indirect (and hence activate cortex and thalamus), will drive glutamatergic synapse formation in the striatum. Collateral connections among MSNs[20] refine BG activity and may contribute to these effects. Such activity-dependent processes may be essential for refining locomotion and reward-based behavior.

These mechanisms are fundamentally distinct from those believed to underlie topographic organization of sensory cortices during postnatal development. In these cortical areas, waves of neural activity pass information about sensory maps from one stage of processing to the next[28,29] and these mappings are translated into synaptic connectivity through spike timing-dependent plasticity rules[30]. In contrast, striatal inputs from widespread cortical areas show only modest topographic organization. Instead of sensory maps, synaptic networks throughout the cortex-BG-thalamus loop are thought to reflect parallel, segregated loops of mixed inhibitory and excitatory projections. Here we show that activity propagates through cortex-BG-thalamus circuits to specify synaptic networks based on the balanced output of direct and indirect pathways in a manner that can, through positive feedback, select for recurrent closed loops.

Methods Summary

Viral expression in BAC transgenic mice

Injections of recombinant Cre-On or Cre-Off[24] AAVs were targeted to striatum of D1-Cre, D2-Cre, or Adora-Cre mice. Rbp4-Cre mice were injected in the somatosensory and motor regions of the cortex. Cre-expressing AAV was injected into the striatum of conditional *Slc32a1* or *Ai14-lsl-TdTomato* mice.

Electrophysiology and 2-photon imaging

Whole-cell voltage clamp recordings were obtained from pathway-identified MSNs in acute coronal slices. Cells were filled with Alexa Fluor 594 (10–20 μM) and imaged using two-photon laser-scanning microscope (810–840 nm).

Supplementary Material

Refer to Web version on PubMed Central for supplementary material.

Acknowledgments

We thank Sabatini Lab member for comments on the manuscript; B. Roth, K. Deisseroth, and M. During for hM4D, ChR2, and Cre, respectively, encoding AAV backbone; and C. Gerfen for the Rbp4-Cre mouse line. Confocal imaging was done through the Harvard NeuroDiscovery and Olympus Imaging Centers. This work was supported by grants from NINDS (NS046579, B.L.S); the W.F. Milton Fund Award and the Leonard and Isabelle Goldenson Research Fellowship (Y.K.); and NIH (F31 NS074842) and Shapiro predoctoral fellowship (A.S.).

References

1. Wiesel TN, Hubel DH. Single-cell responses in striate cortex of kittens deprived of vision in one eye. J Neurophysiol. 1963; 26:1003–1017. [PubMed: 14084161]

2. Smith GB, Heynen AJ, Bear MF. Bidirectional synaptic mechanisms of ocular dominance plasticity in visual cortex. Philosophical Transactions of the Royal Society B: Biological Sciences. 2008; 364:357–367.
3. Stephenson-Jones M, Samuelsson E, Ericsson J, Robertson B, Grillner S. Evolutionary conservation of the basal ganglia as a common vertebrate mechanism for action selection. Curr Biol. 2011; 21:1081–1091. [PubMed: 21700460]
4. Yin HH, Knowlton BJ. The role of the basal ganglia in habit formation. Nat Rev Neurosci. 2006; 7:464–476. [PubMed: 16715055]
5. Alexander GE, DeLong MR, Strick PL. Parallel organization of functionally segregated circuits linking basal ganglia and cortex. Annu. Rev. Neurosci. 1986; 9:357–381. [PubMed: 3085570]
6. Nambu A. Somatotopic organization of the primate Basal Ganglia. Front Neuroanat. 2011; 5:26. [PubMed: 21541304]
7. Smith Y, Bevan MD, Shink E, Bolam JP. Microcircuitry of the direct and indirect pathways of the basal ganglia. Neuroscience. 1998; 86:353–387. [PubMed: 9881853]
8. Gerfen CR. The neostriatal mosaic: multiple levels of compartmental organization in the basal ganglia. Annu. Rev. Neurosci. 1992; 15:285–320. [PubMed: 1575444]
9. Albin RL, Young AB, Penney JB. The functional anatomy of basal ganglia disorders. Trends Neurosci. 1989; 12:366–375. [PubMed: 2479133]
10. Kelly RM, Strick PL. Macro-architecture of basal ganglia loops with the cerebral cortex: use of rabies virus to reveal multisynaptic circuits. Prog Brain Res. 2004; 143:449–459. [PubMed: 14653187]
11. Alexander GE, Crutcher MD. Functional architecture of basal ganglia circuits: neural substrates of parallel processing. Trends Neurosci. 1990; 13:266–271. [PubMed: 1695401]
12. Kravitz AV, et al. Regulation of parkinsonian motor behaviours by optogenetic control of basal ganglia circuitry. Nature. 2010; 466:622–626. [PubMed: 20613723]
13. Ferguson SM, et al. Transient neuronal inhibition reveals opposing roles of indirect and direct pathways in sensitization. Nat Neuroscience. 2010; 14:22–24.
14. Cho J, West MO. Distributions of single neurons related to body parts in the lateral striatum of the rat. Brain Res. 1997; 756:241–246. [PubMed: 9187338]
15. Tong Q, Ye C-P, Jones JE, Elmquist JK, Lowell BB. Synaptic release of GABA by AgRP neurons is required for normal regulation of energy balance. Nat Neurosci. 2008; 11:998–1000. [PubMed: 19160495]
16. McIntire SL, Reimer RJ, Schuske K, Edwards RH, Jorgensen EM. Identification and characterization of the vesicular GABA transporter. Nature. 1997; 389:870–876. [PubMed: 9349821]
17. Wojcik SM, et al. A shared vesicular carrier allows synaptic corelease of GABA and glycine. Neuron. 2006; 50:575–587. [PubMed: 16701208]
18. Gong S, et al. A gene expression atlas of the central nervous system based on bacterial artificial chromosomes. Nature. 2003; 425:917–925. [PubMed: 14586460]
19. Taverna S, Ilijic E, Surmeier DJ. Recurrent collateral connections of striatal medium spiny neurons are disrupted in models of Parkinson's disease. J Neurosci. 2008; 28:5504–5512. [PubMed: 18495884]
20. Sohal VS, Zhang F, Yizhar O, Deisseroth K. Parvalbumin neurons and gamma rhythms enhance cortical circuit performance. Nature. 2009:1–5.
21. Nimchinsky EA, Sabatini BL, Svoboda K. Structure and function of dendritic spines. Annu Rev Physiol. 2002; 64:313–353. [PubMed: 11826272]
22. Somogyi P, Bolam JP, Smith AD. Monosynaptic cortical input and local axon collaterals of identified striatonigral neurons. A light and electron microscopic study using the Golgi-peroxidase transport-degeneration procedure. J Comp Neurol. 1981; 195:567–584. [PubMed: 6161949]
23. Tepper JM, Sharpe NA, Koós TZ, Trent F. Postnatal development of the rat neostriatum: electrophysiological, light- and electron-microscopic studies. Dev Neurosci. 1998; 20:125–145. [PubMed: 9691188]

24. Saunders A, Sabatini B. An expanded toolkit of cre-sensitive adeno-associated viral vectors to deliver fluorophore and optogenetic constructs in vivo. In Preparation.

25. Rogan SC, Roth BL. Remote Control of Neuronal Signaling. Pharmacological Reviews. 2011; 63:291–315. [PubMed: 21415127]

26. Krashes MJ, et al. Rapid, reversible activation of AgRP neurons drives feeding behavior in mice. J. Clin. Invest. 2011; 121:1424–1428. [PubMed: 21364278]

27. Kwon H-B, Sabatini BL. Glutamate induces de novo growth of functional spines in developing cortex. Nature. 2011; 474:100–104. [PubMed: 21552280]

28. Meister M, Wong RO, Baylor DA, Shatz CJ. Synchronous bursts of action potentials in ganglion cells of the developing mammalian retina. Science. 1991; 252:939–943. [PubMed: 2035024]

29. Triplett JW, et al. Retinal input instructs alignment of visual topographic maps. Cell. 2009; 139:175–185. [PubMed: 19804762]

30. Bi G, Poo M. Synaptic modification by correlated activity: Hebb's postulate revisited. Annu. Rev. Neurosci. 2001; 24:139–166. [PubMed: 11283308]

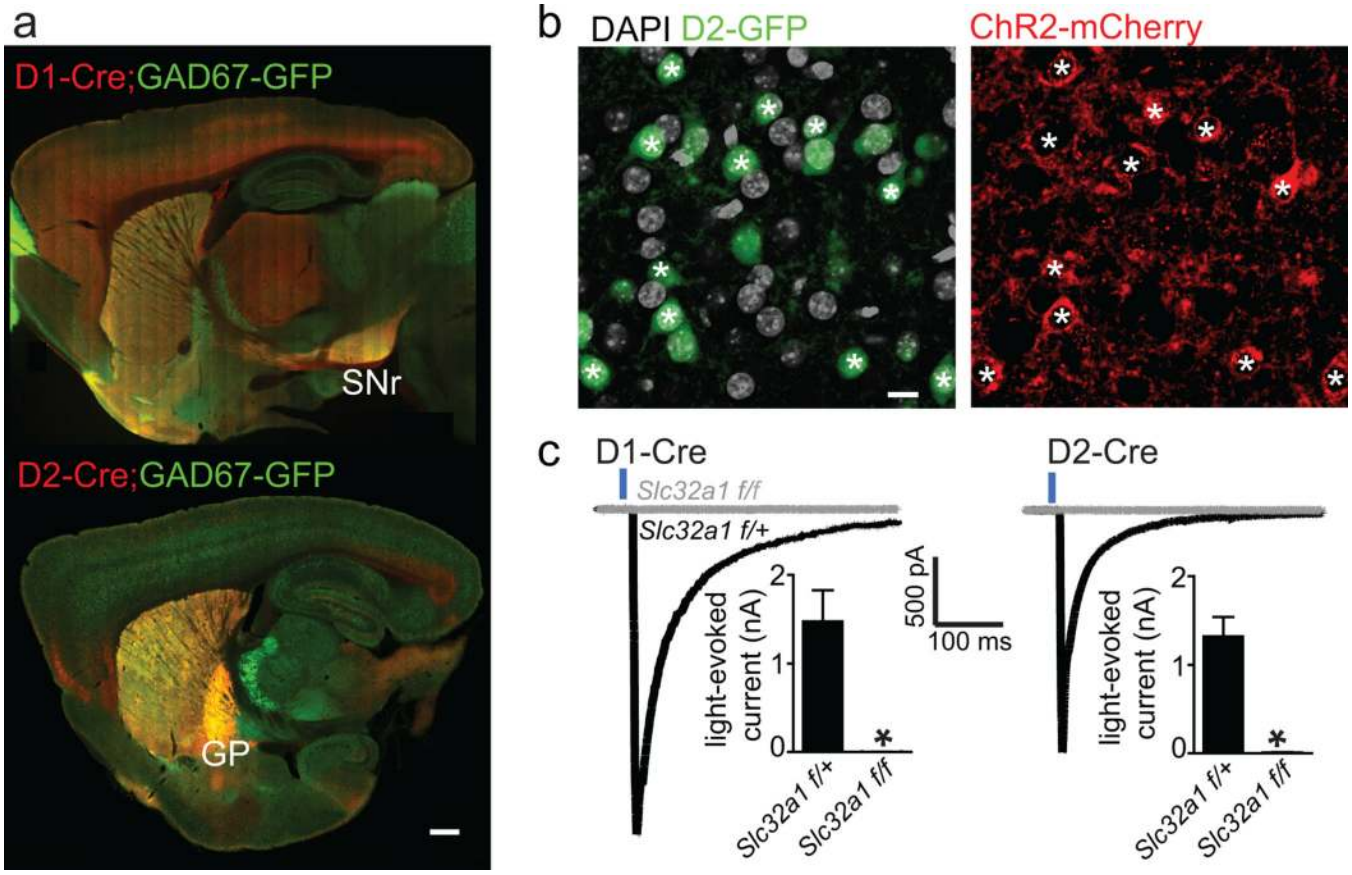

Figure 1. Conditional knock out of *Slc32a1* from direct or indirect pathway MSNs abolishes GABAergic output

a. Cre expression driven by *Drd1a* (D1-Cre, *top*) and *Drd2* (D2-Cre, *bottom*) BACs was visualized via activation of TdTomato in a reporter mouse. Red fluorescence reveals expression throughout striatum and in axons in expected target nuclei of direct and indirect pathway MSNs (SNr and GP, respectively). Green fluorescence reflects expression of a GAD67-GFP that reports GABAergic neurons. As seen in the red channel, there is diffuse cortical expression of Cre in the D1-Cre mice; however, this occurs in non-GABAergic neurons as noted by the lack of overlap with GFP fluorescence (see Supplementary Figure 2 for complete anlaysis). Scale bar: 500 μm.

b. AAV DIO-ChR2-mCherry injected into the striatum of a mouse carrying D2-Cre and D2-GFP transgenes shows ChR2-mCherry labeling in GFP^+ cells, indicating pathway specific conditional expression of the virally encoded protein. ChR2-mCherry-expressing somata are marked with an asterisk and represent over 2/3 of the GFP^+ MSNs in the area of dense infection. ChR2-mCherry was never observed in D2-GFP^- MSNs in these mice. Scale bar: 10 μm.

c. Voltage-clamp recordings from ChR2-$mCherry^-$ MSNs demonstrate GABAergic synaptic currents evoked by 2 ms-long pulses of 473 nm light that stimulates neighboring ChR2-$mCherry^+$ MSNs. Example currents from MSNs in D1-Cre (*left*) and D2-Cre (*right*) mice that were either homozygous (gray, $Slc32a1^{f/f}$) or heterozygous (black, $Slc32a1^{f/+}$) for the *Slc32a1* conditional allele are shown. GABAergic currents are inward due to high intracellular Cl^- concentration. *Insets*, graphs of average peak current amplitudes evoked in animals of each genotype. * indicates $p<0.05$ for comparison of $Slc32a1^{f/+}$ and $Slc32a1^{f/f}$ data. Error bars: SEM

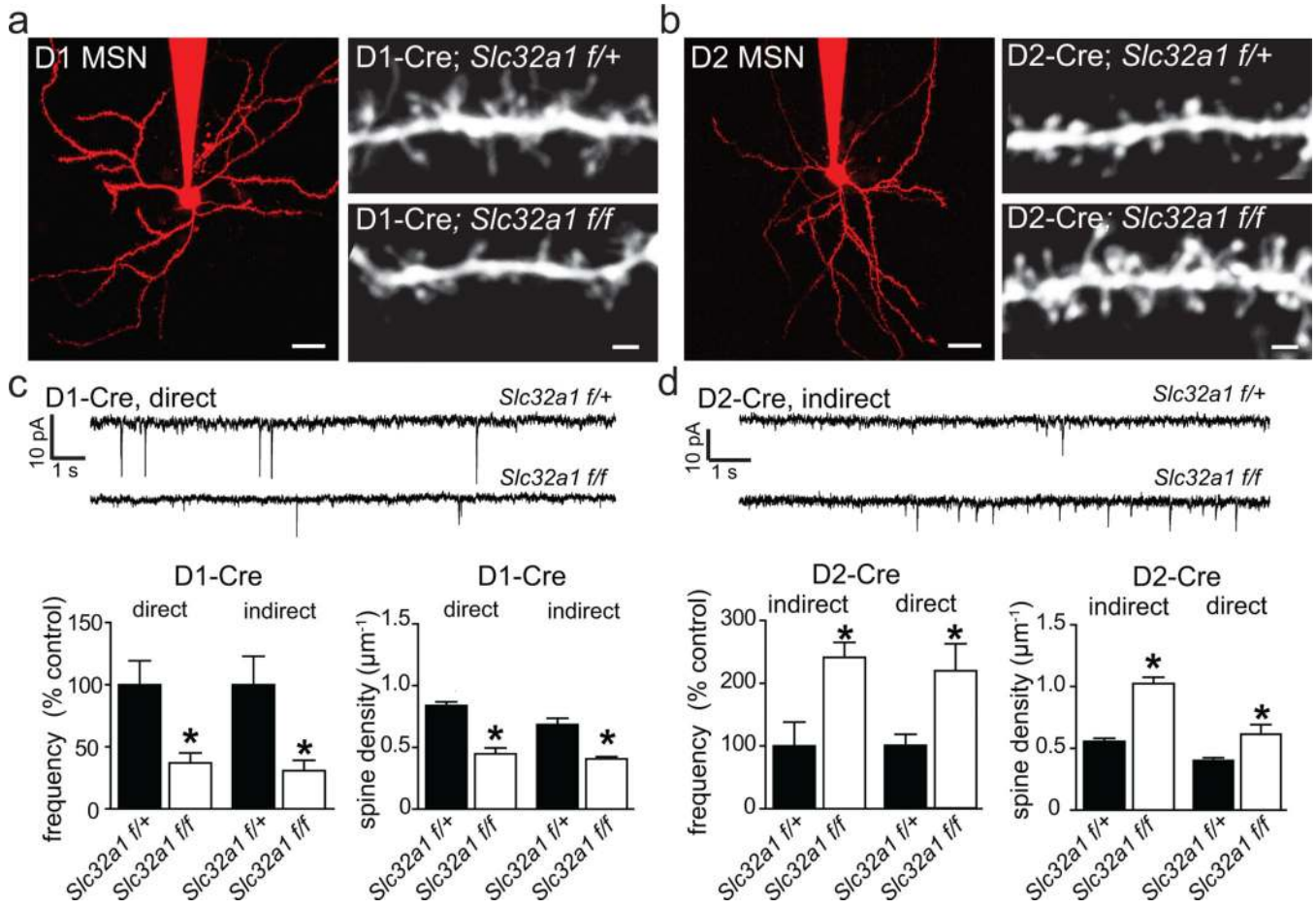

Figure 2. Conditional knock out of *Slc32a1* in direct and indirect pathway MSNs results in opposing changes to excitatory synapse number

a. *left*, 2PLSM image of a direct pathway *Slc32a1*$^{f/+}$ MSN filled with Alexa Fluor 594 through the recording pipette during whole-cell voltage-clamp analysis of mEPSCs. *right*, At a higher magnification, dendritic spines are visible. Examples of a dendrite from a control direct pathway MSN (*top*) and of a less spiny dendrite from a direct pathway MSN of a *Slc32a1* null sibling (*bottom*) are shown. Scale bars: 20 μm, 2 μm.

b. As in (**a**), but illustrating the increase in dendritic spine density seen with silencing of indirect pathway MSNs.

c. Examples and summary of frequencies of mEPSCs in direct pathway *Slc32a1* null mice and their heterozygous sibling controls. Preventing GABA release from direct pathway MSNs reduced mEPSCs frequency, compared to direct pathway MSNs in *Slc32a1*$^{f/+}$ sibling controls (*top*). Summary graph illustrates the decrease in direct and indirect pathway MSNs that were paralleled by differences in the density of dendritic spines. * indicates $p<0.05$ for comparison of *Slc32a1*$^{f/+}$ and *Slc32a1*$^{f/f}$ data.

d. As in (**c**) for indirect pathway mutants indicating that preventing GABA release from indirect pathway MSNs increased mEPSC frequency and dendritic spine density in indirect and direct pathway MSNs. * indicates $p<0.05$ for comparison of *Slc32a1*$^{f/+}$ and *Slc32a1*$^{f/f}$ data. Error bars: SEM

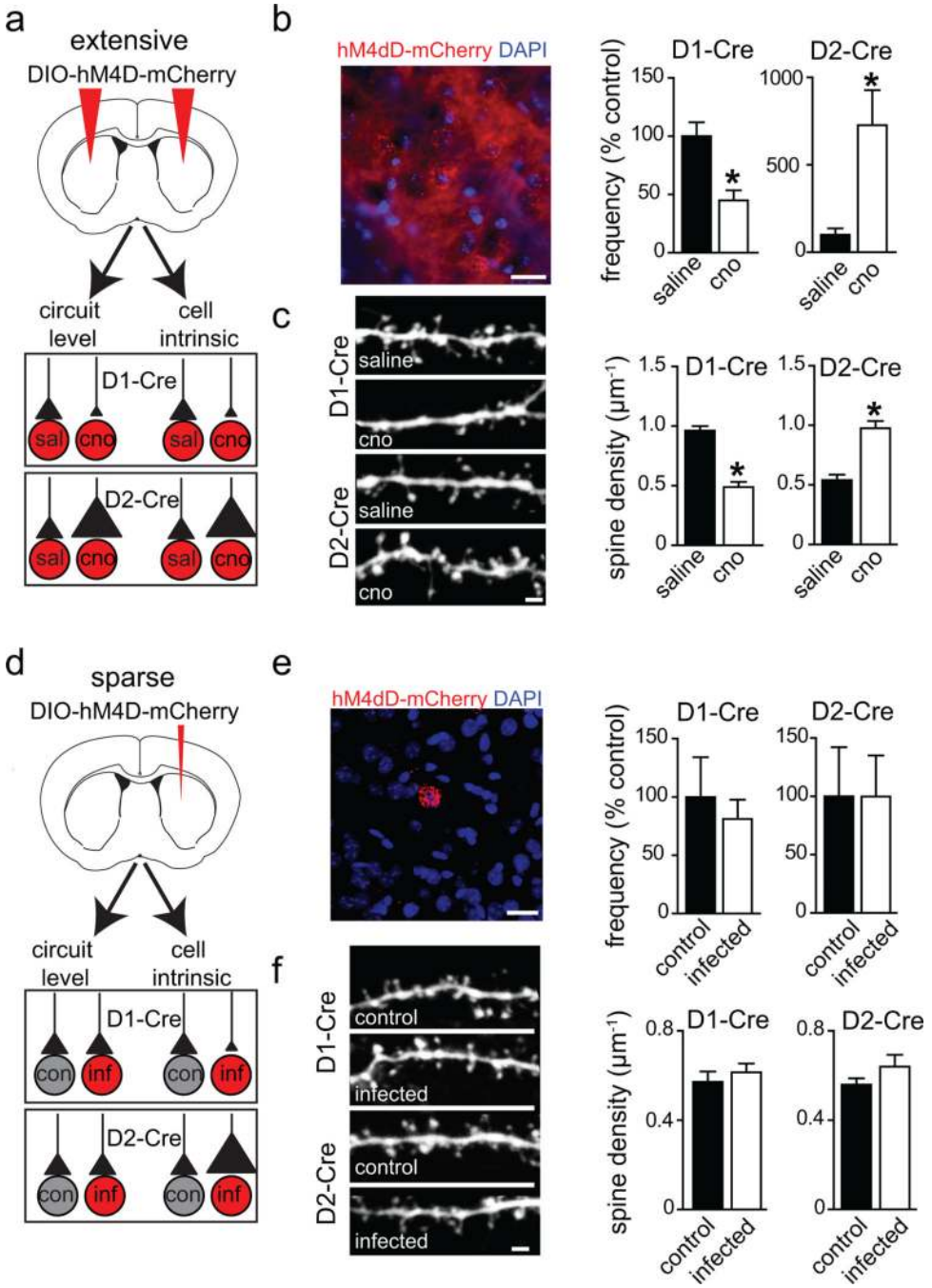

Figure 3. ***In vivo*, developmentally-restricted postnatal manipulation of activity in direct and indirect pathway MSNs results in opposing changes to excitatory synapse number**

a. Schematic of experimental design and hypotheses for changes in excitatory synapse number induced by extensive and bilateral expression of hM4D in direct or indirect pathway MSNs and subsequent injections of cno or saline. Widespread inhibition of direct pathway MSN firing with cno is expected to decrease excitatory synapse number, whether circuit level or cell-intrinsic mechanisms dictate corticostriatal synaptogenesis. The converse is expected for widespread inhibition of indirect pathway MSNs.

b. *left*, hM4D-mCherry^{+} MSNs in tissue densely infected with hM4D-encoding AAV (mCherry, red; DAPI, blue). Scale bar: 20 μm. *right*, Summary data demonstrate that *in vivo*

manipulation of neuronal activity in direct or indirect pathway MSNs in the time window of excitatory synaptogenesis led to opposing changes in excitatory synapse number. Decreased mEPSC frequency was observed in cno-treated D1-Cre mice, whereas mEPSC frequency was enhanced in cno-treated D2-Cre mice, compared to respective saline-injected controls. * indicates $p<0.05$ for the comparison of same pathway MSNs from saline and cno-injected mice.

c. *left top*, 2PLSM images of a dendrite from a direct pathway MSN in a saline-injected mouse and a less spiny dendrite from a cno-injected sibling. Scale bar: 2 μm. *left bottom*, Images showing an example of increased spine density in indirect pathway MSNs of cno-treated animals compared to saline controls. *right*, Summaries of spine density in cno- and saline-treated animals demonstrating the opposite sign changes resulting from inhibition of the direct or indirect pathway. * indicates $p<0.05$ for the comparison of same pathway MSNs from saline and cno-injected mice.

d. Schematic of experimental design and hypotheses for possible changes in excitatory synapse number induced by sparse and unilateral expression of hM4D in direct or indirect pathway MSNs and subsequent injections of cno. Manipulation of activity in a small subset of neurons is not expected to engage circuit-wide mechanisms regulating synapse numbers. In contrast, unknown cell-intrinsic mechanisms could regulate the number of synapses formed onto the manipulated neurons, compared to same pathway uninfected MSNs.

e. *left*, Confocal image showing an hM4D-mCherry expressing MSN in a sparse injection configuration (mCherry, red; DAPI, blue). Scale bar: 20 μm. *right*, With sparse activity manipulations, no differences in mEPSC frequency were observed in either direct or indirect pathway infected, compared to uninfected, MSNs.

f. *left top*, 2PLSM images of a dendrite from control or neighboring hM4D-expressing direct pathway MSN. Scale bar: 2 μm. *left bottom*, Images of spiny dendrites from control or neighboring hM4D-expressing indirect pathway MSN. *right*, Summary graph shows that inhibiting activity of a sparse subset of MSNs does not alter dendritic spine density in manipulated direct or indirect pathway neurons. Error bars: SEM

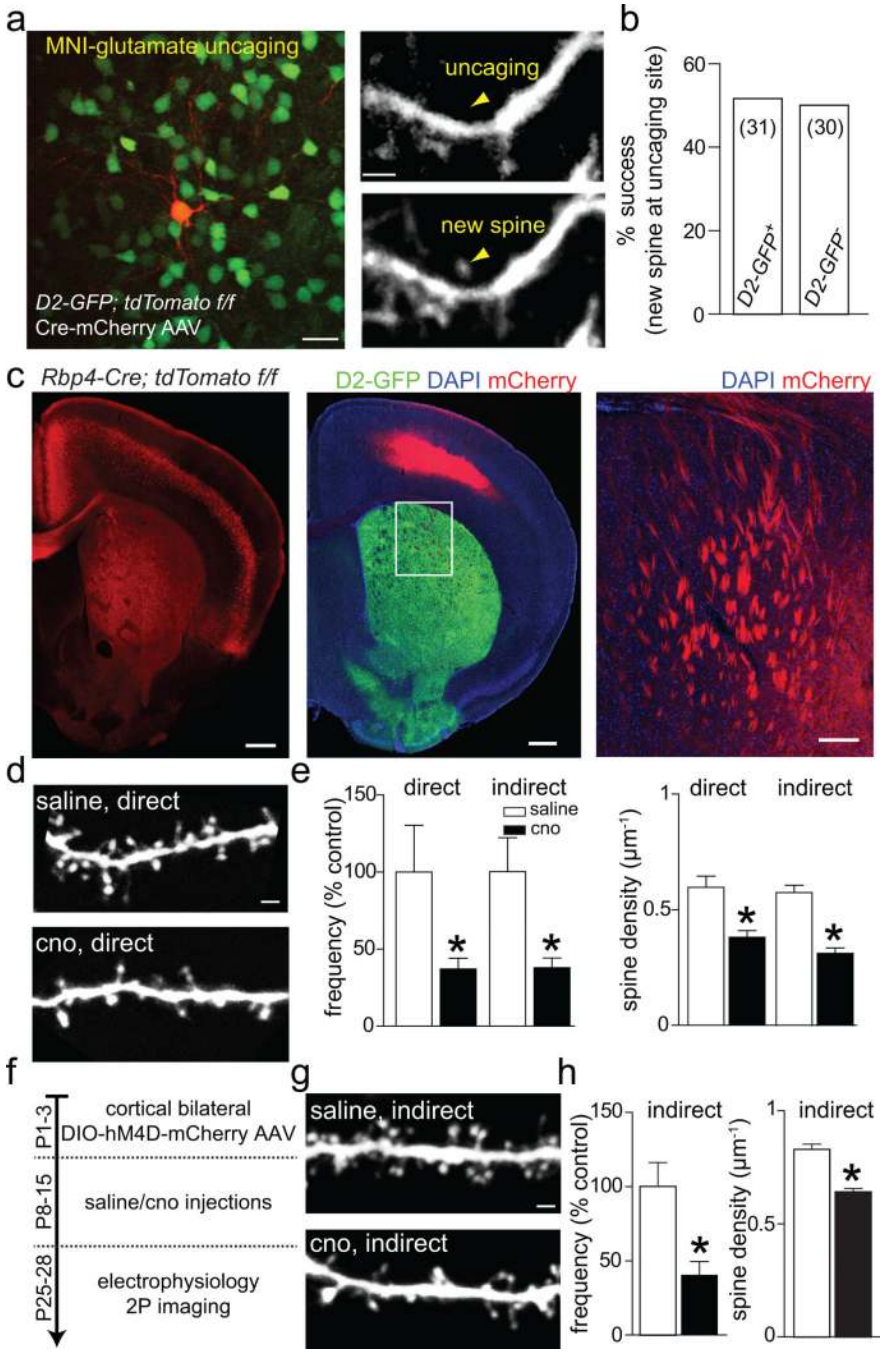

Figure 4. Corticostriatal activity drives synaptogenesis in MSNs

a. Focal release of glutamate is sufficient to trigger *de novo* spinogenesis in MSNs. 2PLSM image of a tdTomato (red) and GFP (green) expressing MSNs in a *D2-GFP*; *tdTomato*$^{f/f}$ mouse sparsely injected with Cre-mCherry encoding AAV at P0. Imaging was performed in an acute slice of striatum at P10. Scale bar: 20 µm. *right*, higher magnification image of a dendrite before (*top*) and after (*bottom*) triggering new spine growth. Scale bar: 2 µm. The stimulation protocol consisted of 40 uncaging pulses directed at the indicated spot (arrow) with 15 mW of 720 nm light measured at the objective back aperture.

b. Summary graph demonstrating ~50% success rate in generating new spines with glutamate uncaging in direct and indirect pathway MSNs at P8-11.
c. *left*, Cre expression driven by an *Rbp4* BAC (Rbp4-Cre) targets Cre to corticostriatal projection neurons. Red fluorescence from a TdTomato reporter allele is present in deep layer cortical neurons and densely labels axons throughout striatum. Scale bar: 500 μm. *middle*, AAV DIO hM4D-mCherry injected into the cortex of a mouse carrying Rbp4-Cre and D2-GFP transgenes shows strong red fluorescence in deep layer somata in cortex and green fluorescence in striatum. Scale bar: 500 μm. *right*, Red channel, higher magnification view of boxed area in the center panel shows extensive hM4D-mCherry labeling of corticostriatal axons.
d and **e**. *In vivo* inhibition of Rbp4-Cre neurons expressing hM4D during the window of excitatory synaptogenesis leads to a decrease in excitatory synapse number for both direct and indirect pathway MSNs. **d**. 2PLSM images of a dendrite from a direct pathway MSN in a saline-injected mouse and a less spiny dendrite from a cno-injected littermate. Scale bar: 2 μm. **e**. Summary data showing a decrease in direct and indirect pathway MSN mEPSC frequency (*left*) and spine density (*right*) for cno-treated mice versus saline treated littermates.
f – h. hM4D/cno-dependent decreases in MSN excitatory synapse number persist into early adulthood. **f**. Timeline for experiments. **g**. 2PLSM images of dendrites from indirect pathway MSNs from sibling mice in their early adulthood (P25- 28) after treatment with cno or saline during the time window for excitatory synaptogenesis (P8-15). **h**. Summary data showing that decreases in mEPSC frequency (*left*) and spine density (*right*) persist into early adulthood. Error bars: SEM